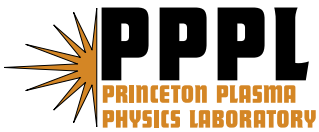# Princeton Plasma Physics Laboratory

PPPL-

PPPL-

PPPL
PRINCETON PLASMA
PHYSICS LABORATORY

Prepared for the U.S. Department of Energy under Contract DE-AC02-09CH11466.

Princeton Plasma Physics Laboratory
Report Disclaimers

PPPL Report Availability

Princeton Plasma Physics Laboratory:

http://www.pppl.gov/techreports.cfm

Office of Scientific and Technical Information (OSTI):

http://www.osti.gov/bridge

Related Links:

U.S. Department of Energy

Office of Scientific and Technical Information

Fusion Links

Transition to ELM-free improved H-mode by lithium deposition on NSTX graphite divertor surfaces

D.K. Mansfield [a,*], H.W. Kugel [a], R. Maingi [b], M.G. Bell [a], R. Bell [a], R. Kaita [a], J. Kallman [a], S. Kaye [a], B. LeBlanc [a], D. Mueller [a], S. Paul [a], R. Raman [c], L. Roquemore [a], S. Sabbagh [d], H. Schneider [a], C.H. Skinner [a], V. Soukhanovskii [e], J. Timberlake [a], J. Wilgen [b], L. Zakharov [a]

[a] Princeton Plasma Physics Laboratory, Princeton University, Princeton, NJ 08443, United States
[b] Oak Ridge National Laboratory, Oak Ridge, TN 37831, United States
[c] University of Washington, Seattle, WA 98195, United States
[d] Columbia University, New York, NY 10027, United States
[e] Lawrence Livermore National Laboratory, Livermore, CA 94551, United States

ARTICLE INFO

Available online xxxx

PACS:
52.55.Hc
52.55.Fa
52.40.Hf
52.25.−b

ABSTRACT

Lithium evaporated onto plasma facing components in the NSTX lower divertor has made dramatic improvements in discharge performance. As lithium accumulated, plasmas previously exhibiting robust Type 1 ELMs gradually transformed into discharges with intermittent ELMs and finally into continuously evolving ELM-free discharges. During this sequence, other discharge parameters changed in a complicated manner. As the ELMs disappeared, energy confinement improved and remarkable changes in edge and scrape-off layer plasma properties were observed. These results demonstrate that active modification of plasma surface interactions can preempt large ELMs.

© 2009 Elsevier B.V. All rights reserved.

1. Introduction

During H-modes, large edge pressure and current gradients in toroidal fusion devices are thought to drive transient instabilities known as edge localized modes (ELMs) [1]. Numerical simulations have identified peeling and/or ballooning modes as candidate instabilities generating filamentary structures that burst outward across flux surfaces during periodic non-linear growth phases [2,3]. Because ELMs carry a substantial transient heat and particle load into the scrape-off layer (SOL), they will present serious power-handling problems to future fusion devices. For example, the allowable energy loss per ELM in the international thermonuclear experimental reactor was recently revised downward to 0.3% of the plasma stored energy [4].

Hence, active mitigation and suppression of ELMs has been an important international research thrust [5,6]. In the National Spherical Torus Experiment (NSTX), a wide range of ELMs has been observed [7,8]. In particular, ordinary Type I ELMs with individual stored energy reductions of 5–15% are common, as are smaller Type V ELMs [9,10]. This work describes the use of lithium conditioning in which both Types I and V ELMs disappeared, resulting in quiescent ELM-free discharges. Similar ELM disappearance was observed in recent NSTX experiments [11]. Here, however, ELM dis-

appearance was studied in more detail and with more diagnostics. Our more general observation of confinement improvement with lithium has also been reported in other devices [12–15], whereas the use of lithium as a PFC material has also been discussed elsewhere [16,17].

2. Experimental method

Experiments to assess the effects of lithium coatings on ELMs were carried out using an improved generation of the NSTX LIThium EvaporatoR (LITER) and employing new operating procedures [18]. Using recently installed shutters to block Li vapor from the LITER ovens, evaporation into the lower NSTX divertor was suppressed selectively during ∼1 s high-power discharges and the ∼6.5 min He glow conditioning that followed each discharge. Evaporation proceeded, however, for ∼10 min immediately before each high-power discharge. Further, to improve deposition uniformity, LITER was expanded from a single to a dual evaporator system [11]. These new conditioning techniques differed from previous single-oven LITER operation when deposition proceeded continuously, including during both high-power discharges and He conditioning [18]. Using both evaporators, deposition rates as high as 85 mg/min were accomplished.

Initial externally controlled machine parameters in this study were chosen to produce high-recycling, neutral-beam-injection (NBI) heated plasmas with reproducible Type 1 ELMs. These

* Corresponding author.
  E-mail address: dmansfield@princeton.edu (D.K. Mansfield).

experiments were begun after several months of NSTX operation without lithium. Hence, the no-lithium reference discharges taken at the start of these experiments were representative of recycling from the existing boron-treated graphite plasma facing components (PFCs) [19,20].

From previous NSTX experience, ELM disappearance was anticipated shortly after lithium deposition began. The purpose of this work, therefore, was to observe phenomenology of ELM disappearance caused by wall conditioning by introducing lithium slowly into a few discharges held at fixed external parameters.

3. Results

The experiments have documented dramatic decreases in ELM activity with concomitant increases in plasma energy confinement when the NSTX lower divertor PFCs were gradually conditioned over ~25 discharges from lithium-free graphite surfaces to graphite with a thin coating of lithium. This work can be separated into two phases: (a) zero-to-low initial evaporation rates and (b) higher evaporation rates with higher Li accumulation.

3.1. Zero-to-low initial evaporation rates

Shown in Fig. 1 are traces of the D_α radiation emitted from the lower divertor and the plasma stored energy. The data displayed are for a reproducible reference discharge (129019) taken just before lithium deposition began as well as for two of the first five discharges following the start of lithium evaporation (129021 and 129025). Deposition at 8 mg/min from each LITER oven (total: 16 mg/min) began immediately after reference discharge 129020. As seen in Fig. 1, longer discharge durations, resulting from a decrease in inductive flux consumption was an immediate consequence of lithium deposition. Further, an increase in plasma energy confinement was also observed in the first few discharges after the start of lithium conditioning and was accompanied by a modest (~4%) decrease in line-average density.

As indicated by Fig. 1 D_α signals, pronounced changes in ELM frequency or amplitude were not readily apparent during the first two or three post-conditioning discharges. By the fifth discharge

following the start of lithium (129025), however, a clear change in behavior was observed when ELM-free periods appeared intermittently for extended periods of time. It should be noted that an obvious reason for the variability of the duration of these quiescent phases is not evident, i.e., there is no transport or MHD precursor just before the onset of the ELMs that terminate the quiescent phases. An immediate increase in energy confinement when the ELMs disappeared is also evident. Starting when ELM activity is clearly absent ($t \sim 300$ ms) plasma stored energy in 129025 began a pronounced rise that was interrupted shortly before the arrival of a large ELM followed by a compound ELM ($t \sim 430$ ms) which reduced energy confinement. After these events, another ELM-free period began and stored energy began another pronounced rise which continued until ELMs began again at $t \sim 550$ ms. These events are highlighted by arrows in Fig. 1.

The impact of lithium conditioning on ELMs is documented in more detail in Fig. 2. Displayed are D_α signals from $t = 200$–400 ms for a no-lithium reference shot (129019) and for the first five discharges after evaporation began (129021-25). The ELMs can be seen to change slowly over the course of the first few discharges after evaporation began. On the fifth discharge, however, an extended period of quiescent behavior was apparent (also displayed in Fig. 1).

3.2. Higher evaporation rates with higher accumulated lithium

As the experiment progressed, changes in external machine parameters had to be made owing to the pronounced improvements in plasma performance that took place as previously deposited lithium accumulated on the PFCs and as 'new' lithium was deposited at higher rates. In particular, because plasma energy confinement was generally increasing as lithium accumulated at fixed beam power (4 MW), a beta limit ($\beta_N \sim 5.5$) was typically reached early in the discharge and degraded subsequent plasma performance. Further, because plasma line-average density at fixed fuelling rate (49 torr-l/s) was generally decreasing as lithium accumulated, locking of rotating modes was also observed and also degraded plasma performance. Hence, to ameliorate both of these effects simultaneously, NBI power was reduced (to 2 MW) and fuelling was increased (to 58 torr-l/s). As a result, an ELM-free H-mode with improved energy confinement was observed. This is displayed in Fig. 3 where plasma parameters are shown for a no-
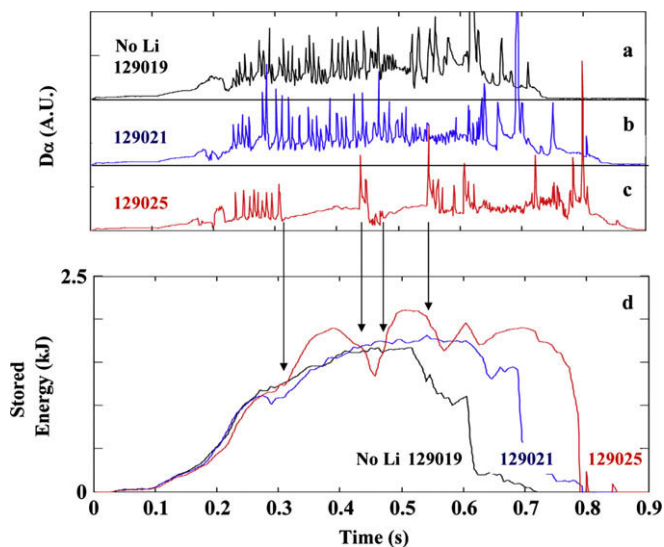

Fig. 1. The D_α (curves a–c) and stored energy traces (curve d) of a no-lithium (129019) as well as the first (129021) and fifth (129025) discharges after lithium evaporation began. ELMs clearly changed during 129025; two ELM-free periods were accompanied by transient increases in energy confinement as indicated by arrows. All D_α data are displayed on identical arbitrary scales.
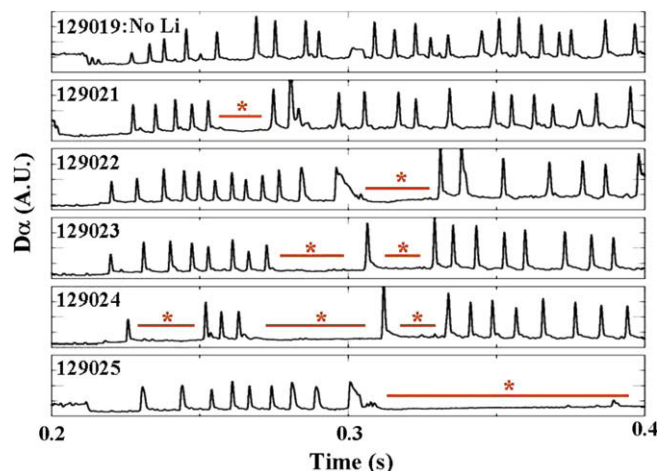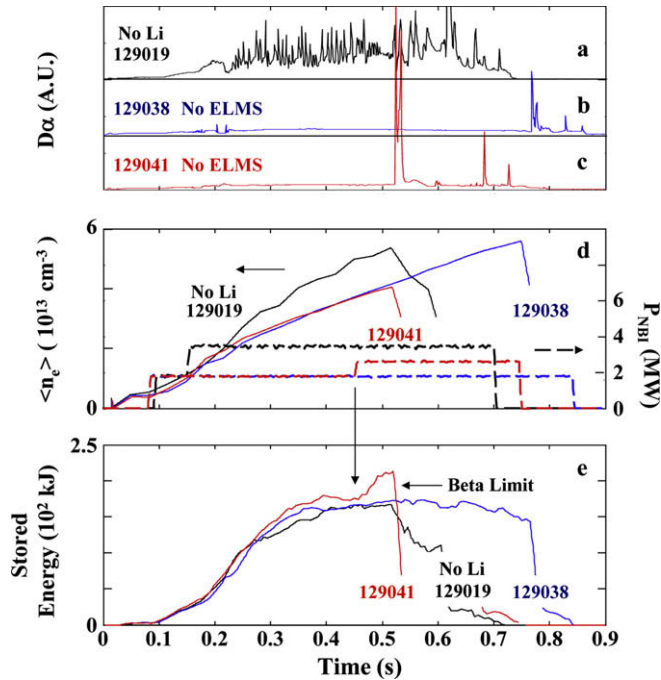

Fig. 2. ELM activity displayed in detail for a no-lithium discharge and for the first five discharges after starting lithium evaporation at a constant 16 mg/min. The total amount of lithium accumulated changed uniformly from 0 to ~800 mg by just before the fifth discharge. All D_α data are displayed on identical arbitrary scales.
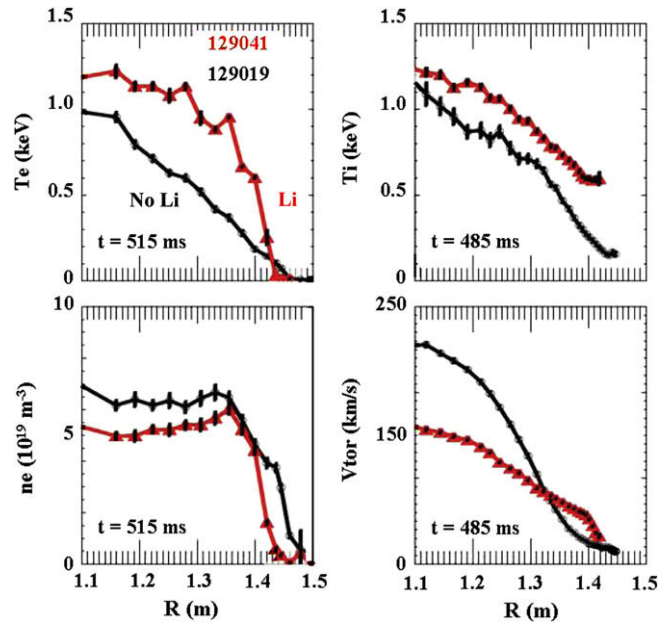
Fig. 3. Plasma parameters of a no-lithium (129019) and two ELM-free discharges (129038 and 129041) that benefitted from both a large lithium accumulation and a high evaporation rate. All D_α data (curves a–c) from these discharges are displayed on identical arbitrary scales. Line-average densities as well as NBI powers are displayed in curve d while the plasma stored energies are shown in curve e. Discharge 129041 was deliberately driven to a beta limit by increasing the NBI power at $t = 450$ ms.

Fig. 4. Kinetic profiles (n_e, T_e, T_i, and V_φ) of an ELMing no-lithium (129019) and an ELM-free discharge (129041, see Fig. 3). Some data are displayed at slightly different times owing to differences of individual diagnostic data collection rates.

Fig. 5. Measured SOL density profiles for an ELMing discharge with a small lithium accumulation (129024) and for the ELM-free discharge (129041) discussed in Figs. 3 and 4 with much higher lithium accumulation.

lithium reference discharge as well as for a discharge with higher fuelling but much lower NBI power (129038). This discharge occurred well after the lithium campaign began and, therefore, received the benefit of a lithium accumulation of 5734 mg of which 767 mg were deposited in the ~10 min preceding this discharge owing to an increased lithium evaporation rate of 70 mg/min. It is noteworthy that 129038 achieved the same stored energy as the reference discharge but required only half the NBI power. Specifically, the energy confinement time relative to the ITER-97L H-mode global scaling increased from about 1.7 to 2.7, i.e., by 60%. This large improvement in energy confinement bears a similarity to the VH-mode in DIII-D [21]; in NSTX discharges, however, a secular increase in radiated power fraction is observed for the longest ELM-free lithium-enhanced discharges, which was absent in the DIII-D VH-mode data.

Also shown in Fig. 3 is the behavior of another discharge (129041) during which NBI power was raised to 3 MW at $t = 450$ ms. This discharge was also ELM-free and remained so even after the increase in NBI heating. An increase in stored energy without any apparent density change was observed during this enhanced heating phase which ended when a global beta limit was reached at ~520 ms. This discharge received the benefit of 8348 mg of accumulated lithium of which 970 mg was deposited in the ~14 preceding minutes at a rate of 70 mg/min.

Shown in Fig. 4 is a comparison of n_e, T_e, T_i, and V_φ profiles from a no-lithium reference discharge and shot 129041 (displayed in Fig. 3). The data are displayed for a time just before the beta limit was reached in 129041 and show pronounced effects of lithium conditioning. Relative to ELM-timing in 129019, the n_e and T_e are just before the onset of a large Type I ELM (from Thomson scattering), whereas the T_i and V_φ are from slightly earlier in the discharge because of the 10 ms averaging window of the charge exchange
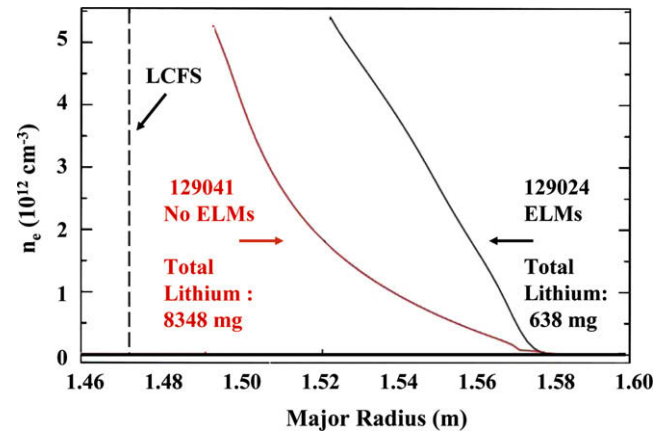
recombination diagnostic. Aside from obvious increases in both $T_i(0)$ and $T_e(0)$, it is clear that extremely large increases occurred at the plasma edge so that edge-pedestal-like features (~600 eV) are apparent in both T_i and T_e. Electron density can also be seen to decrease on either side of the pedestal while the pedestal density at $R \sim 1.35$–1.37 m was unchanged. A pedestal-like feature can also be seen to appear on the edge toroidal rotation while the core rotation dropped. This rotation behavior is not presently understood, but may be related to changes in the radial electric field.

The strong edge modification shown in Fig. 4 was also observed in the plasma SOL. Displayed in Fig. 5 are two edge density profiles measured with an X-mode reflectometer in 129024 during ELM activity and in 129041 with no ELMs [22]. Distinct changes in shape and magnitude of the SOL density indicate strong pumping due to evaporated lithium.

4. Discussion and conclusions

An ELM-free H-mode with improved confinement characteristics was observed, due to lithium coating of the graphite divertor tiles in NSTX. The transition from ELMy to ELM-free H-mode involved neither a gradual increase in ELM period nor a gradual reduction in ELM amplitude. Instead, ELMs in this study disappeared in a series of abrupt intermittent omissions in their growth (highlighted by asterisks Fig. 2). This was particularly clear in 129025 (bottom Fig. 2). The nine ELMs preceding the quiescent period did not exhibit significantly different periods from the nine ELMs seen in the no-lithium discharge at the same time (top panel), nor was the period of these particular nine ELMs (shot 129025) increasing just before the quiescent period. Further, no evidence of decreasing ELM amplitude exists anywhere in the data. Hence, the most obvious manner in which ELMs can be replaced by quiescent behavior (e.g., by decreased ELM amplitude, by decreased ELM frequency, or by a combination of both) was *not* at work in the ELM-free H-mode enabled by lithium conditioning. This simple observation should be incorporated into any theory describing ELMS modification by PFC conditioning [23,24].

Immediate increases in stored energy during ELM-free periods are obvious in Figs. 1 and 3. Further, in all cases, the absence of ELMs, whether transient or lasting for the entire discharge duration, was accompanied by pronounced increases in energy confinement. This observation, when considered together with the profound changes in edge and SOL parameters (Figs. 4 and 5) caused by a thin layer of lithium, indicate that lithium conditioning of divertor PFCs can be a powerful tool to achieve ELM-free discharges with improved plasma performance. Although these discharges are transient in nature, techniques to trigger small ELMs to create quasi-steady discharges are presently being developed.

References

[1] J.W. Connor, R.J. Hastie, H.R. Wilson, R.L. Miller, et al., Phys. Plasmas 5 (1998) 2687.
[2] H.R. Wilson, P.B. Snyder, G.T.A. Huysmans, et al., Phys. Plasmas 9 (2002) 1277.
[3] P.B. Snyder, H.R. Wilson, J.R. Ferron, et al., Phys. Plasmas 9 (2002) 2037.
[4] (e.g. discussed in) A. Loarte et al., Plasma Phys. Control. Fus. 45 (2003) 15 (The acceptable ITER ELM energy loss was recently revised downward and does not appear in a refereed article).
[5] C.M. Greenfield, K.H. Burrell, J.C. DeBoo, et al., Phys. Rev. Lett. 86 (2001) 4544.
[6] T.E. Evans, R.A. Moyer, P.R. Thomas, et al., Phys. Rev. Lett. 92 (2004) 235003.
[7] M. Ono, S.M. Kaye, Y.-K.M. Peng, et al., Nucl. Fus. 40 (2000) 557.
[8] R. Maingi, C.E. Bush, E.D. Fredrickson, et al., Nucl. Fus. 45 (2005) 1066.
[9] R. Maingi, S.A. Sabbagh, C.E. Bush, et al., J. Nucl. Mater. 337–339 (2005) 727.
[10] R. Maingi, K. Tritz, E. Fredrickson, et al., Nucl. Fus. 45 (2005) 264.
[11] H.W. Kugel, M.G. Bell, J.-W. Ahn, et al., Phys. Plasmas 15 (2008) 056118.
[12] D.K. Mansfield, D.W. Johnson, B. Grek, et al., Nucl. Fus. 41 (2001) 1823.
[13] R. Majeski et al., Phys. Rev. Lett. 97 (2006) 075002.
[14] J. Sanchez et al., I-02, these Proceedings, doi:10.1016/j.jnucmat.2009.01.224
[15] S.V. Mirnov et al., Fus. Eng. Des. 65 (2003) 455.
[16] G. Mazzitelli et al., P1-49, these Proceedings.
[17] Y. Hirooka et al., Nucl. Fus. 46 (2006) S56.
[18] H.W. Kugel et al., P2-58, these Proceedings, doi:10.1016/j.jnucmat.2009.01.262
[19] J. Winter, J. Nucl. Mater. 162 (1989) 713.
[20] H.W. Kugel et al., J. Nucl. Mater. 290–293 (2001) 1185.
[21] G.L. Jackson et al., Phys. Rev. Lett. 67 (1991) 3098.
[22] J.B. Wilgen et al., Rev. Sci. Instrum. 77 (2006) 10E933.
[23] L.E. Zakharov et al., J. Nucl. Mater. 363–365 (2007) 453.
[24] S.Yu. Medvedev et al., Plasma Phys. Control. Fus. 48 (2006) 927.